AIAA JOURNAL
Vol. 44, No. 4, April 2006

Modeling of Energy Backscatter via an Algebraic Subgrid-Stress Model

S. Bhushan,* Z. U. A. Warsi,† and D. K. Walters‡
Mississippi State University, Starkville, Mississippi 39762

In large-eddy simulation, the subgrid-stress model is included to represent the energy-transfer mechanisms between the resolved and unresolved scales of motion. Although most models represent forward scatter (dissipation) of energy, they fail to account for backscatter properly. The algebraic model, obtained directly from the closure of the subgrid stresses, has an additional term over the mixed model that accounts for the backscatter of energy explicitly. This model has been previously documented in the open literature and shows promising results in accounting for the subgrid-scale energy-transfer mechanisms. Detailed documentation is provided of the backscatter capability of the algebraic model, for a series of test cases including isotropic turbulence, plane channel flow, and two free shear flows. The model performace in predicting turbulent flow quantities is also compared with commonly used subgrid-stress models and with the available direct-numerical-simulation data.

Nomenclature

B	=	backscatter, $\langle \alpha_2 \Delta^2 [(\text{grad}\,\hat{\boldsymbol{u}})^T \cdot \text{grad}\,\hat{\boldsymbol{u}}] : \hat{\boldsymbol{D}} \rangle$
c_b	=	backscatter coefficient B/ϵ
c_f	=	forward scatter coefficient F/ϵ
c_L	=	Leonard's dissipation coefficient L/ϵ
$\hat{\boldsymbol{D}}$	=	rate-of-strain tensor, $\frac{1}{2}[\text{grad}\,\hat{\boldsymbol{u}} + (\text{grad}\,\hat{\boldsymbol{u}})^T]$
F	=	forward scatter, $\langle 2C_s^2 \Delta^2 [2\hat{\boldsymbol{D}} : \hat{\boldsymbol{D}}]^{1/2} \hat{\boldsymbol{D}} : \hat{\boldsymbol{D}} \rangle$
L	=	Leonard's dissipation, $-\langle \alpha_1 \Delta^2 [\text{grad}\,\hat{\boldsymbol{u}} \cdot (\text{grad}\,\hat{\boldsymbol{u}})^T] : \hat{\boldsymbol{D}} \rangle$
$T(k)$	=	transfer spectra, $\int\int_s \hat{\tau}_{ij} \hat{D}^*_{ij}\, \text{d}s(k)$
Δ	=	filter width
ϵ	=	dissipation, $-\boldsymbol{\tau} : \hat{\boldsymbol{D}}$
$\int\int_s \text{d}s(k)$	=	integral over a surface of sphere of radius k
$\langle\,\rangle$	=	volume averaging

Superscripts

$*$	=	complex conjugate
$\hat{}$	=	Fourier components

I. Introduction

OVER the past few decades, large-eddy simulation (LES) has emerged as a powerful tool for simulation of turbulent flows. However, application of LES to complex engineering problems requires accurate modeling of subgrid stresses (SGS). The main effect of the subgrid stresses is to transfer energy between resolved and unresolved scales of motion. This occurs bidirectionally, where transfer of energy from resolved scales to subgrid scales is referred to as forward scatter and from subgrid scales to resolved scales as backscatter. An SGS model that adequately provides net dissipation (forward scatter) can produce acceptable results for the mean quantities, but cannot accurately predict the turbulent structure of the flow.[1–3] Several recent efforts have been focused on development of models capable of producing backscatter, but the complex form of the models often renders them unusable for engineering applications. The purpose of this paper is to present the capability of a previously documented algebraic model[4,5] in predicting backscatter in a variety of flowfields.

The energy backscatter phenomenon is known to occur through the cross and Reynolds stresses.[4] The cross stresses represent the interaction of scales of motion across the cutoff wave number leading to energy transfer to resolved scales. The limiting case of these stresses is referred to as local interaction, which leads to a divergence of forward and backscatter transfers at cutoff, observed both numerically[6,7] and analytically.[4,8] However, these transfers are an artifact of the filtering operation rather than an intrinsic feature of fluid turbulence.[3] Schilling and Zhou[7] emphasized the importance of modeling the divergence of forward scatter and backscatter near cutoff, which has received much attention in LES community. The representation of such divergence can be obtained far more easily in wave-number space than in physical space.[3,8] The other mechanism of energy transfer is by the Reynolds stresses, which are an intrinsic feature of the turbulent flow, and must be reproduced by the SGS modeling independent of filtering and defiltering of the velocity field.[8] The backscatter via this term can be estimated analytically through the nonlocal interactions.[8,9] Schumann[10] provided a better estimate, for the entire range of Reynolds interaction, by imposing structural equilibrium. The simplistic approach for the SGS is to model the net forward and backscatter by the Reynolds and cross stresses together. Although such assumption does not require forward and backscatter divergence at cutoff, it does require proper modeling of backscatter, which is not localized only to the cutoff scales. The algebraic model coefficients, used in this paper, are obtained based on this assumption.[4]

The most common approach for SGS modeling is to use an eddy-viscosity model such as the Smagorinsky model (SM), which also forms the basis of several more models.[11] Some of the drawbacks of the original SM have been overcome by the dynamic adjustment of the model coefficient, referred to as the dynamic Smagorinsky model (DSM).[12] DSM has been shown to be successful in predicting mean turbulent quantities[13] and providing backscatter in an averaged sense.[14] A priori analysis[15] shows that the (mis)alignment of the SGS tensor with the mean strain-rate tensor plays a decisive role in the occurrence of backscatter. The coefficient of a linear model cannot be optimized to achieve this effect because by definition stress and strain-rate tensors are aligned in these models. Inclusion of desirable backscatter with an eddy-viscosity model has been achieved stochastically by many researchers.[10,16] In spectral space such an approach can be adjusted to provide proper backscatter both at lower wave-numbers and at cutoff.[8] However, stochastic modeling represents a more traditional picture of the turbulence

Received 26 April 2005; revision received 23 September 2005; accepted for publication 27 September 2005.

*Postdoctoral Research Associate, SimCenter Engineering Research Center. Member AIAA.

†Emeritus Professor, Department of Aerospace Engineering. Associate Fellow AIAA.

‡Assistant Professor, Department of Mechanical Engineering. Member AIAA.

as "random" motion and does not account for the organized vortical structures associated with the backscatter phenomenon,[3,17] hence, employing stochastic forcing as a reliable model remains doubtful.[18]

It has been reported that scale-similarity models can provide backscatter of energy in a deterministic fashion.[13,19] This inherent advantage of the scale-similarity term has inspired variants such as gradient,[13,20] subfilter scale,[21] and deconvolution[22,23] models. As noted by Bhushan and Warsi[4] Carati et al.,[21] the scale-similar terms are closely related to the modified Leonard's stresses. The Taylor's series expansion of the modified Leonard's term,[24] and deconvolution are identical up to the second-order terms,[23] which are usually retained. It has been observed that the modified Leonard's stresses correlate well with cross-stress term,[25,26] and therefore scale-similar terms represent backscatter via such correlations.[1] However, the analysis of the modified Leonard's term suggests that it leads to net forward scatter,[4,27] which is one reason why these models do not provide sufficient backscatter in LES calculations.[28] Further, for sharp spectral filters the modified Leonard's term vanishes, resulting in zero backscatter for these models, inconsistent with the flow physics. These models still lack proper modeling of the backscatter mechanism.[29]

The preceding class of models is usually combined with an eddy-viscosity term to obtain a mixed model (MM).[13,22] The eddy-viscosity term therefore accounts for both the Reynolds and cross stresses. Because these interactions lead to both forward and backscatter energy transfers,[9] which are completely different phenomena from each other, it has been suggested that they should be modeled independently.[26] The mixed model therefore appears to lack a complete modeling of the subgrid-scale energy-transfer mechanisms. To remedy this, some researchers have adopted independent modeling of backscatter along with the MM (for example, Horiuti,[25] inspired from the correlation between the modified Leonard's and cross stresses, and others,[2,30] but only on a heuristic basis). Moreover, these models involve additional model coefficients, which are computed dynamically, leading to additional computational expense. They also suffer from numerical instability issues.[25] Domaradzki and Adams[22] discuss a direct modeling approach, where the subgrid velocity field is estimated from the resolved scales. Such methods are theoretically capable of directly accounting for both forward and backscatter energy transfer, but require higher numerical resolution and are computationally expensive relative to more traditional stress tensor models.

The purpose of this paper is to document the capability of a constant coefficient algebraic subgrid-stress model[4] (AM) in independently predicting backscatter of energy for an array of LES test cases. The AM is obtained directly from the closure of the transport equation for the subgrid stresses.[4] It has been shown previsously (compare to Bhushan and Warsi[4]) that AM resolves the stress anistropy or the (mis)alignment of the SGS and strain-rate tensor better than the MM. The AM has an additional term over the MM that provides backscatter in the canonical approach. In essence, the AM provides independent modeling of the forward and backscatter resulting from the net effect of Reynolds' and cross stresses. A similar term as in the AM is also present in the Lagrangian-averaged Navier–Stokes (LANS)-α model,[31] obtained from a completely different approach. Recently, Geurts and Holm[32] documented the backscatter capability of this term in mixing layer simulations. The AM has constant model coefficients computed based on analytic energy transfer estimates,[4] which are used in the all of the simulations presented herein. In this work, the capability of the algebraic model in depicting the backscatter phenomenon is reported for a number of well-understood test cases. These include isotropic decaying and forced turbulence, wall-bounded channel flows over a range of Reynolds numbers, and free-shear flows such as a temporally developing planar jet and mixing layer.

II. Algebraic Model

In LES the governing equations for the resolved scale motion $\hat{\boldsymbol{u}}$ are obtained by filtering (applied implicitly in this paper) the Navier–Stokes equations. For incompressible flows, they are

$$\operatorname{div}\hat{\boldsymbol{u}} = 0$$

$$\frac{\partial\hat{\boldsymbol{u}}}{\partial t} + (\hat{\boldsymbol{u}}\cdot\operatorname{grad})\,\hat{\boldsymbol{u}} = -\operatorname{grad}\hat{p} + \nu\operatorname{div}(\operatorname{grad}\hat{\boldsymbol{u}}) - \operatorname{div}(\boldsymbol{\tau}) \quad (1)$$

where $\boldsymbol{\tau} = \widehat{\boldsymbol{u}\boldsymbol{u}} - \hat{\boldsymbol{u}}\hat{\boldsymbol{u}}$ is the subgrid-stress tensor, which must be modeled for closure of the equations. The AM is obtained from the second-order deductive iteration of the constitutive equations for the algebraic subgrid-stress transport equation. The anisotropic component of the AM is thus obtained as (compare to Bhushan and Warsi[4] for details)

$$\boldsymbol{\tau} = -2C_s^2\Delta^2[2\hat{\boldsymbol{D}}:\hat{\boldsymbol{D}}]^{\frac{1}{2}}\hat{\boldsymbol{D}} + \alpha_1\Delta^2\Big[\operatorname{grad}\hat{\boldsymbol{u}}\cdot(\operatorname{grad}\hat{\boldsymbol{u}})^T - \tfrac{1}{3}(\operatorname{grad}\hat{\boldsymbol{u}}:\operatorname{grad}\hat{\boldsymbol{u}})\boldsymbol{I}\Big]$$
$$-\alpha_2\Delta^2\Big[(\operatorname{grad}\hat{\boldsymbol{u}})^T\cdot\operatorname{grad}\hat{\boldsymbol{u}} - \tfrac{1}{3}(\operatorname{grad}\hat{\boldsymbol{u}}:\operatorname{grad}\hat{\boldsymbol{u}})\boldsymbol{I}\Big] \quad (2)$$

Readers are referred to Warsi[5] for the index notation of the model. The eddy-viscosity model (SM) has only the first term in Eq. (2). The second term in the model is the leading term in the Taylor's series expansion of the modified Leonard's stress.[24] Although varying in details, a similar term is also obtained from the deconvolution approach.[23] As discussed by Carati et al.,[21] this term has close ties with the scale similarity[13] and subfilter stresses.[21] The MM[1,28] consists of the first two terms of the AM. As evident, the AM has an additional term that (for positive model coefficients) yields negative dissipation (i.e., backscatter) for the canonical case.[4] A similar term is also present in the LANS-α model,[31] and its backscatter capability was recently reported by Geurts and Holm.[32] Such terms cannot be obtained by Taylor's series expansion or upon deconvolution. The AM, in contrast, provides explicit modeling of the different sugrid-scale energy-transfer mechanisms naturally.

The unknown model coeficients need to be adjusted such that the closure of Eq. (2) with the rate-of-strain tensor produces the proper amount of dissipation. The estimates of the amount of dissipation can be obtained in the canonical case, that is, homogeneous isotropic turbulence with infinite inertial subrange. The coefficients can be evaluated such that the first, second, and third terms account for the c_f, c_L, and c_b fractions of total dissipation ϵ, respectively. The steps involved in the estimates of these transfer coefficients are discussed in Bhushan and Warsi.[4] Interested readers can also refer to Appendix A in Ref. 4 for estimates of terms resulting from the closure of Eq. (2) with $\hat{\boldsymbol{D}}$ in the canonical case. The computations to determine the coefficients were based on implicitly applied Gaussian filtering to the Navier–Stokes (NS) equations as in Eq. (1). The MM coefficients can be evaluated similarly such that the eddy-viscosity term leads to the combined effect of forward and backscatter ($c_f - c_b$). The model coefficients thus computed are presented in Table 1. For the SM the recommended value of the coefficient is $C_s^2 = 0.03$ for isotropic turbulence[33] and 0.01 for the channel[34] and free-shear flow cases,[28] which are used in this paper. The DSM coefficients are computed following Lilly[12] using Simpson's rule with averaging performed along the homogeneous directions and with secondary filter width twice equal to the grid scale.[34]

Table 1 Model coefficients of the SGS models

Model	C_s^2	α_1	α_2
Smagorinsky	0.03 (0.01)	——	——
Mixed	0.0162	1/12	——
Algebraic	0.0213	1/12	0.03364

III. Isotropic Turbulence

The numerical simulation of isotropic turbulence allows an assessment of the capability of the AM terms in depicting the subgrid-scale energy-transfer mechanisms. Calculations have been performed for isotropic decaying and forced isotropic turbulence in a periodic cubic box of side 2π. The governing equations are solved using a pseudospectral code, where $\frac{3}{2}$ rule is used to remove the aliasing error along homogeneous directions, and a second-order

Runge–Kutta scheme is used for time evolution.[33] The initial velocity fields for these cases are generated following Rogallo.[35] The random phases adjust themselves to physically realistic values in the beginning of the simulation, resulting in an initial transient period. The DSM coefficient stabilizes to $C_s^2 = 0.03$ (for filter width ratio of 2) (Ref. 33) at the end of the transient phase, which is identical to that of SM. Therefore simulations using DSM are not presented. The AM and the MM are based on Gaussian filtering, and the filter width Δ was chosen such that the transfer function at cutoff wave number k_c is $G(k_c) = 0.8$ (Ref. 36). Further, AM and MM simulations were started with filtered (Gaussian) velocity profiles and the results defiltered for comparison with SM results.

A. Decaying Turbulence

The first simulations were performed based on the Comte-Bellot and Corrsin (CBC) experiment,[37] which corresponds to Reynolds number Re equal to 1346 (Ref. 33), with three grid resolution levels: 32^3, 48^3, and 64^3. The direct-numerical-simulation (DNS) grid requirement for this case is 192^3 (based on three times the Kolmogrov's length scale); thus, the grid scales are six, four, and three times larger than the DNS scales for the coarse, medium, and fine grid, respectively. The complete set of results for this case is presented in Bhushan and Warsi[4]; only the key results are reproduced here. Figure 1a compares the evolution of the resolved scale kinetic energy for each of the models on the coarse grid. (The other grid resolutions showed similar results.) The no-model case (NM) does not dissipate energy properly and leads to energy pile up across the cutoff wave number as seen in Fig. 1b. It can be observed that the SM is more dissipative than the AM, followed by the MM. Comparison of the energy spectrum (Fig. 1b) shows that the AM has more energy in the higher wave-number range (because of the explicit backscatter) than the MM and the SM, thereby predicting more energy overall.

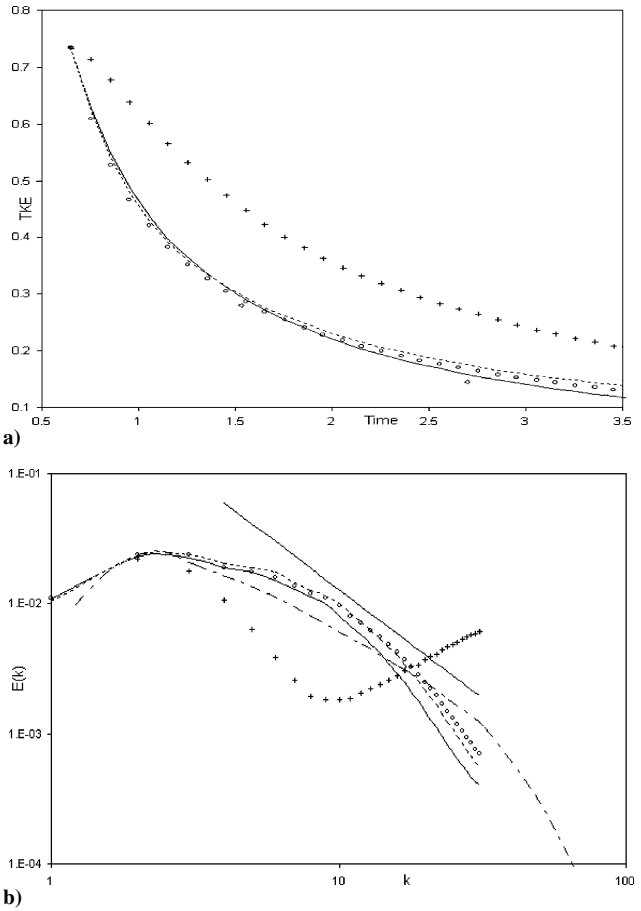

Fig. 1 Isotropic decaying turbulence, Re = 1346: a) resolved scale kinetic energy (TKE) evolution on 32^3 grid and b) energy spectra compared with $k^{-5/3}$ spectra on 64^3 grid: ——, SM; – – –, MM; ○, AM; +, no model; and ◇ or — - —, experimental.[37]

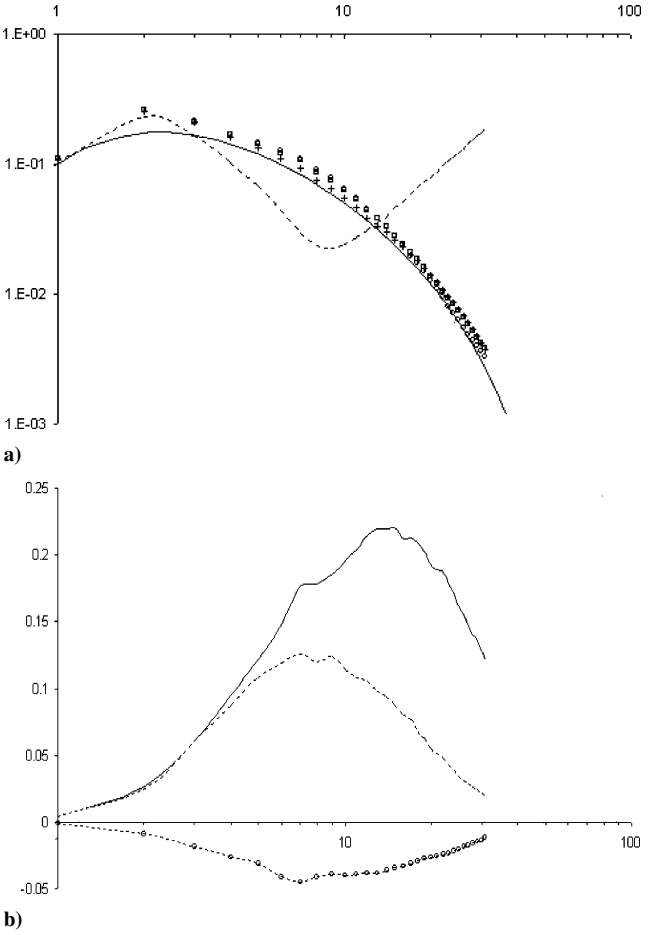

Fig. 2 Isotropic decaying turbulence, $Re = 2.472 \times 10^4$: a) energy spectra compared with experimental result at x/M = 48; ——, experimental[29]; – – –, NM; ○, SM; □, MM; and +, AM; b) transfer spectral of AM [Eq. (2)] terms: ——, first term (eddy viscosity); – – –, second term (Leonard's); and –○–, third term (backscatter).

The second test case considered is based on the experiments of Kang et al.,[29] which corresponds to higher $Re = 2.472 \times 10^4$. The DNS grid requirements are therefore much higher, that is, 384^3 based on scale resolution of four times the Kolmogrov's length scale. The simulation is performed here on a single grid of 64^3, which leads to a grid six times coarser than the DNS requirements. All of the models show similar dissipation rates in good comparison with the experimental results. The energy spectra presented in Fig. 2a show that all of the models predict the spectra in good agreement with the experimental data; however, the AM is slightly better in the intermediate wave-number range. Similar behavior was observed at other experimental locations. Figure 2b shows the transfer spectra of the AM terms. It is apparent that the energy input by the backscatter term occurs throughout the resolved scales of motion. The input peaks at an intermediate wave number and then decreases across the cutoff. The peak of the Leonard's dissipation is approximately at the same location as that of the backscatter. The energy transfer by the eddy-viscosity term peaks closer to the cutoff wave number, but drops sharply near the cutoff wave number. As the cross-stress terms are not explicitly accounted for, finite forward and backscatter at cutoff is expected.[7] The energy-transfer coefficients obtained for both Reynolds-number cases and all grid resolutions are close to each other. Although their values vary from the canonical case as shown in Table 2, they are within acceptable limits.

B. Forced Turbulence

Statistically stationary homogeneous turbulence has been simulated by forcing energy injection into the lower wave-number modes of the velocity fields. Simulations were performed for the 32^3, 48^3, and 64^3 grid resolutions with two forcing functions. The Reynolds number of the flow was assumed to be infinite so that the

Table 2 Estimate of energy-transfer coefficients by the algebraic model terms

Test case	c_f	c_L	c_b
Canonical case	0.736	0.44	0.176
Isotropic decaying	0.82	0.325	0.143
Forced isotropic	0.8	0.335	0.135
Channel flow (away from the wall)	0.95	0.45	0.4
Free-shear flow	0.854	0.245	0.1

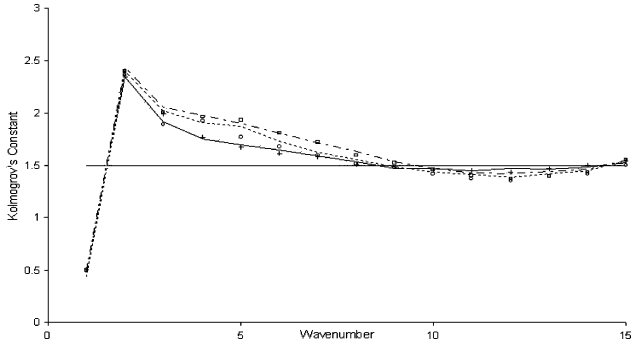

Fig. 3 Kolmogrov's constant on 32^3 grid case: – – –, SM ($\epsilon = 0.1$); ○, SM ($\epsilon = 0.2$); —·—, MM ($\epsilon = 0.1$); □, MM ($\epsilon = 0.2$); ——, AM ($\epsilon = 0.1$); and +, AM ($\epsilon = 0.2$).

energy transfer takes place only by the SGS terms. The initial energy spectrum used for the simulation corresponds to the Kolmogrov's $-\frac{5}{3}$ spectrum. Further details of the simutaions are presented in Bhushan and Warsi.[4] Figure 3 compares the Kolmogrov's constant, $C_k = E(k)\epsilon^{-2/3}k^{5/3}$, predicted by the SGS models for the 32^3 grid. All of the simulations show that C_k varies around 1.5, as observed by other authors.[16] The AM predicts the flattest C_k profile followed by the SM and MM. The turbulent cascade develops independently of the amount of energy injected into the system. The results on other grids showed a similar nature (for which figures are not presented). In this case, too, the AM provides energy backscatter independently via the third term in Eq. (2). The energy-transfer coefficients thus obtained are close to those from the isotropic decaying case, as shown in Table 2.

IV. Channel Flows

The second case considered is the numerical simulation of the plane channel flow performed at three Reynolds numbers (Re_τ: based on friction velocity u_τ and half-channel-width δ) 180, 395, and 590 referred to as cases 1, 2, and 3, respectively. These flows have been studied in detail using DNS[38] and provide a detailed investigation of the backscatter capability of the AM in wall-bounded flows. The governing equations (1) are solved using the Fourier–Galerkin method in the homogeneous streamwise and spanwise directions and a second-order finite difference scheme in the wall-normal direction. Time advancement is performed using the fractional step method with a modified third-order Runge–Kutta step for explicit terms and second-order Crank–Nicholson scheme for implicit terms. The nonlinear terms in the SGS are treated explicitly. The computations are performed on a rectangular staggered grid, which is uniform in the spanwise and streamwise directions and hyperbolically stretched along the wall-normal direction. The aliasing error along the homogeneous directions is removed by using the $\frac{3}{2}$ rule. The channel flow is governed by the constant pressure gradient, which appears as a forcing term in Eq. (1) chosen appropriately to balance the targeted wall shear stress (compare to Chang[34] for the details of numerical method). The simulation parameters of these cases and detailed results are presented in Bhushan and Warsi.[4] A summary of the results is presented here. As DSM is found to be sufficiently accurate in the channel flow case[1]; AM results for all three cases are compared with DSM. However, for the lowest-Reynolds-number case simulations using SM and no-model (NM) were also performed for comparison. An additional simulation, which is referred to as AM^b, using AM was performed on a grid refined along the homogeneous directions for cases 1 and 2.

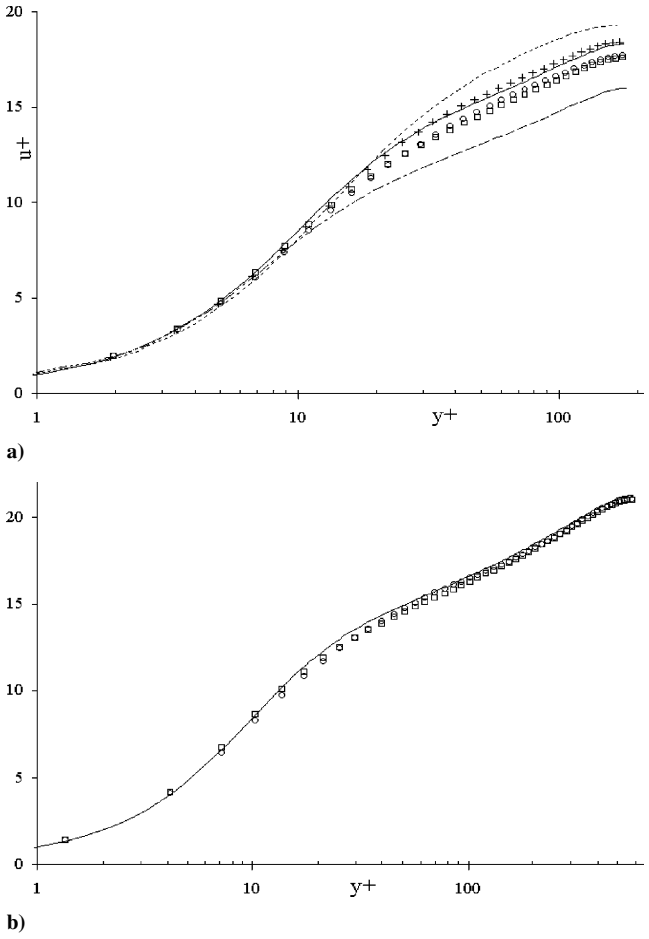

Fig. 4 Mean streamwise velocity profile: a) case 1 and b) case 3; – · –, NM; – – –, SM; □, DSM; ○, AM^a; +, AM^b; and ——, DNS.[38]

Channel flow involves flow inhomogeneity in the wall-normal direction, which is not accounted for by the constant model coefficients such as in SM and AM.[39] Therefore a Van Driest-type damping function[20] is used along with the filter width Δ, which is obtained based on the geometric average of mesh spacing, that is, $\Delta = [\Delta_x \Delta_z \Delta_y(y)]^{1/3}$. The DSM coefficient, obtained by averaging along homogeneous directions, does not require an ad hoc damping function. The simulations were started with an artificial velocity field obtained by imposing random phase perturbations over the fully developed mean channel flow quantities. The phases adjusted themselves initially leading to a transient period. To obtain a better statistical sample of the turbulent quantities, running time averages were performed after the statistically steady state was reached. (In this section, $\langle\cdot\rangle$ implies both plane and time-averaged quantity.)

Mean skin-friction coefficients obtained in all of the AM and DSM simulations agree well (within 1–2%) with the target values, but SM underestimates its value considerably (about 5%). As seen in Fig. 4 for case 1, both the DSM and the AM^a simulations produce good results in the sublayer, buffer-layer, and log-layer regions for the mean streamwise velocity; however, the Smagorinsky model deviates from the log profile. The AM^b simulation predicts slightly lower wall stresses thereby predicting a larger intercept in the log layer. This profile matches exactly with the DNS data, where the larger intercept is regarded as the low-Reynolds-number effect.[38] The NM case underestimates the mean velocity significantly. In cases 2 and 3 the mean velocity profile from both the AM and DSM are in good agreement with the DNS results, and grid refinement does not seem to have a substantial effect.

Figure 5 presents the Reynolds shear stress obtained in the numerical simulations. Again, both the AM and DSM predict the stresses in excellent agreement with the DNS results, whereas SM underpredicts its value. The fine grid simulation has the same behavior as that

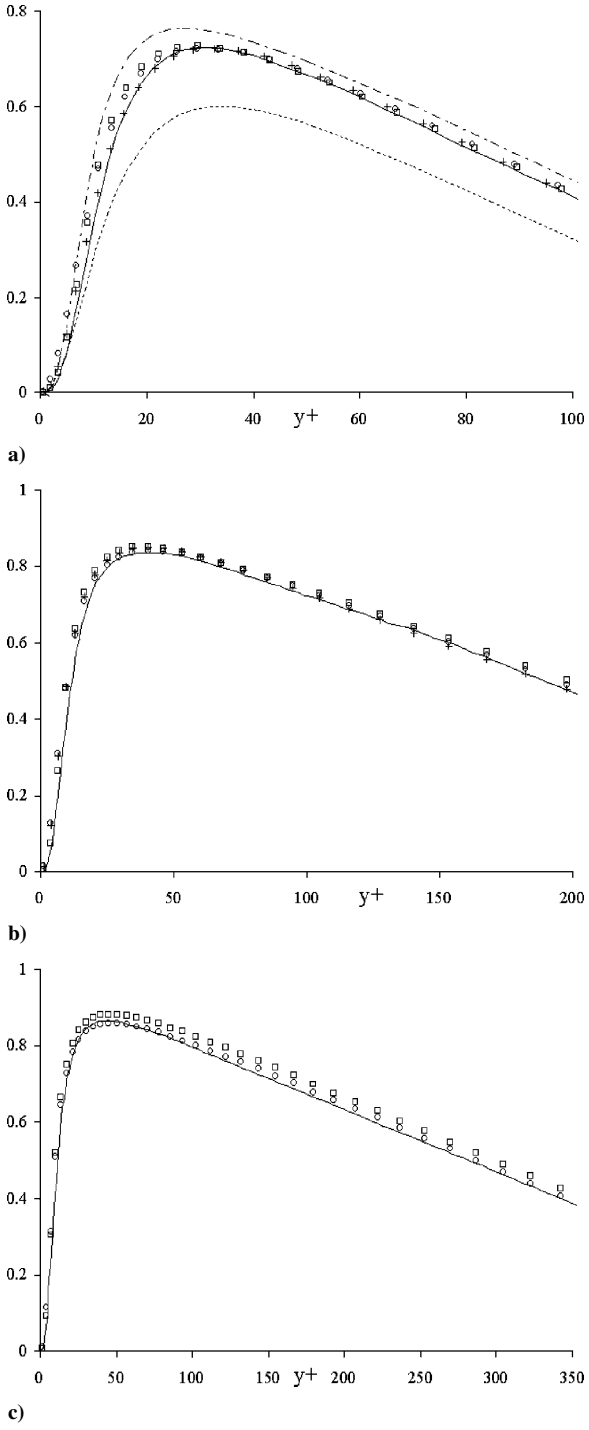

Fig. 5 Reynolds stress ($\langle -u'v' \rangle + \langle \tau_{uv} \rangle$) compared with DNS result: a) case 1, b) case 2, and c) case 3. Same keys as in Fig. 3.

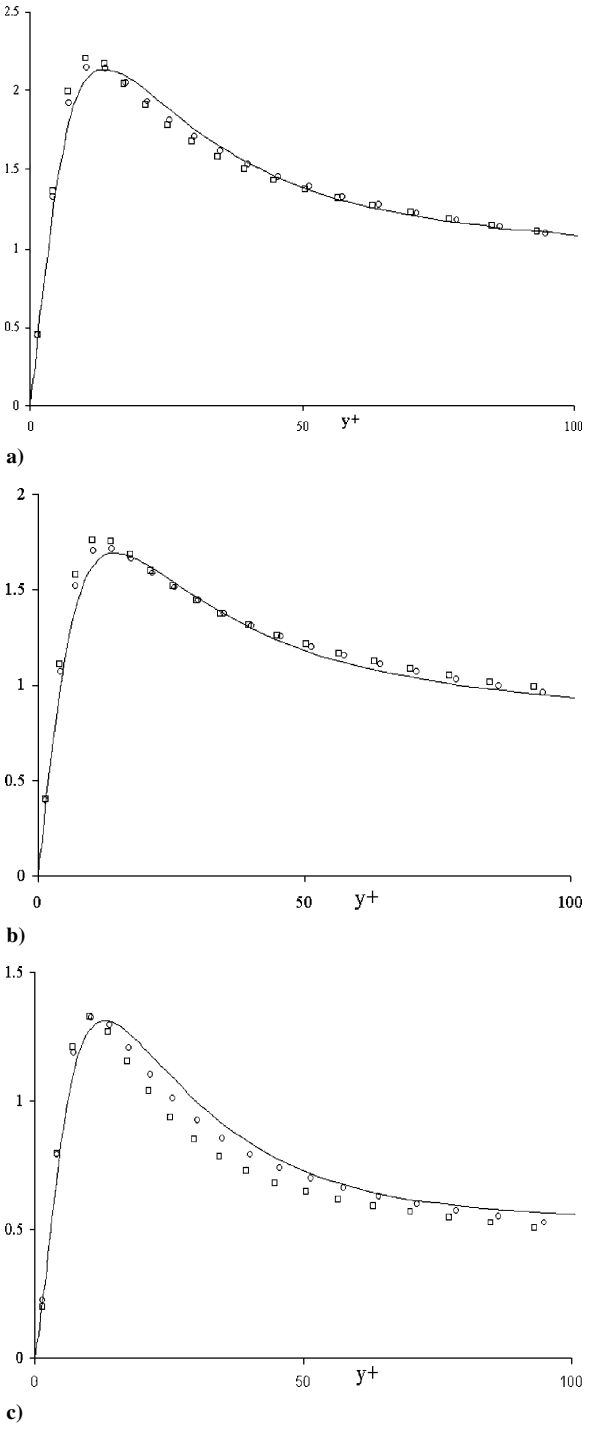

Fig. 6 RMS values of a) streamwise velocity fluctuations u', b) spanwise velocity fluctuations v', and c) wall-normal velocity fluctuation w' for case 3. Same keys as in Fig. 3.

of the coarse-grid simulation. However, results of AM are closer to the DNS compared to the DSM values, especially for case 3.

Figure 6 presents the anisotropic turbulence intensities for case 3 (accounts for the contributions from the resolved fluctuations and the subgrid stresses[23]), which are compared with the anisotropic component of the DNS data. For the low-Reynolds-number case AM predicts the peak of turbulence intensities better than DSM, but deviates in the region away from the wall, where DSM performs better. SM overpredicts the intensities, whereas NM case is underpredictive. The results on a finer grid AM^b show improvement over the coarse-grid results by predicting a better profile. In cases 2 and 3, the AM performs much better than the DSM, and the results are closer to the DNS. DSM fails to accurately predict the peak of the velocity fluctuations in these cases as well. In case 3, DSM underestimates the spanwise velocity fluctuation considerably as seen in Fig. 6c. Overall, the AM performs better than DSM especially for the higher-Reynolds-number cases.

Qualitative nature of the higher-order statistics, that is, skewness and flatness, of the flow are compared for case 2 in Figs. 7 and 8. For the streamwise skewness AM performs better followed by DSM and SM. Similarly, the normal velocity skewess peak is better predicted by AM than either the DSM or SM results. The spanwise velocity skewness for all of the models varies slightly but stays close to zero as expected because of the flow symmetry along the spanwise direction.[17] For the flatness values it is expected that numerical values should be underpredictive[40]; however, both DSM and SM overpredict the streamwise values near the wall, whereas the AM

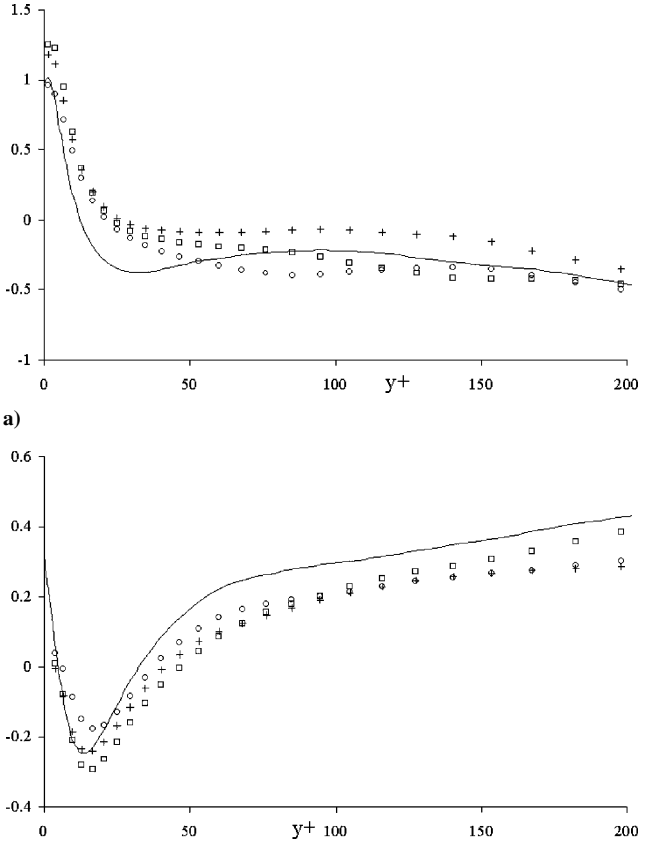

Fig. 7 Skewness factor for case 2: a) $S(u')$ and b) $S(v')$. Same keys as in Fig. 3.

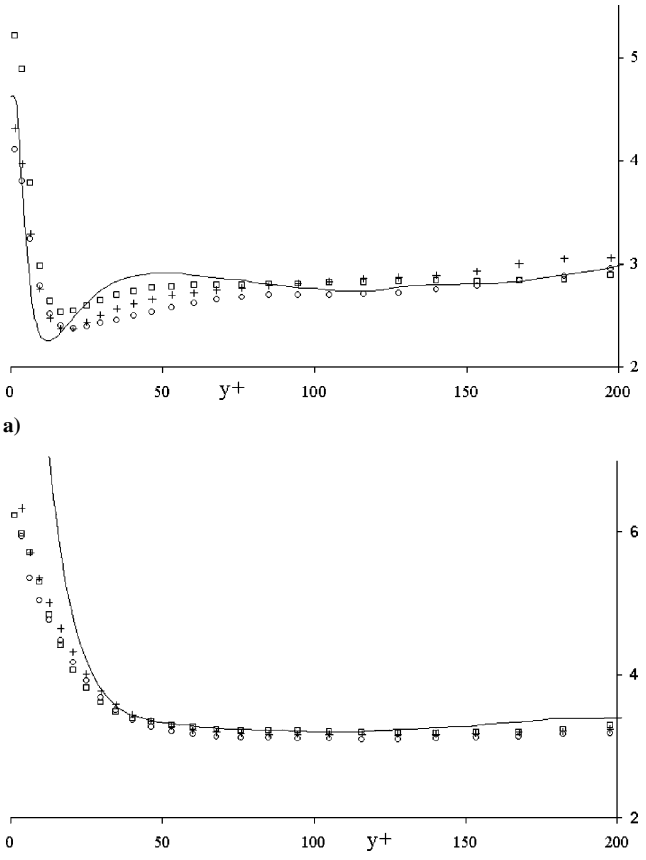

Fig. 8 Flatness factor for case 2: a) $F(u')$ and b) $F(v')$. Same keys as in Fig. 3.

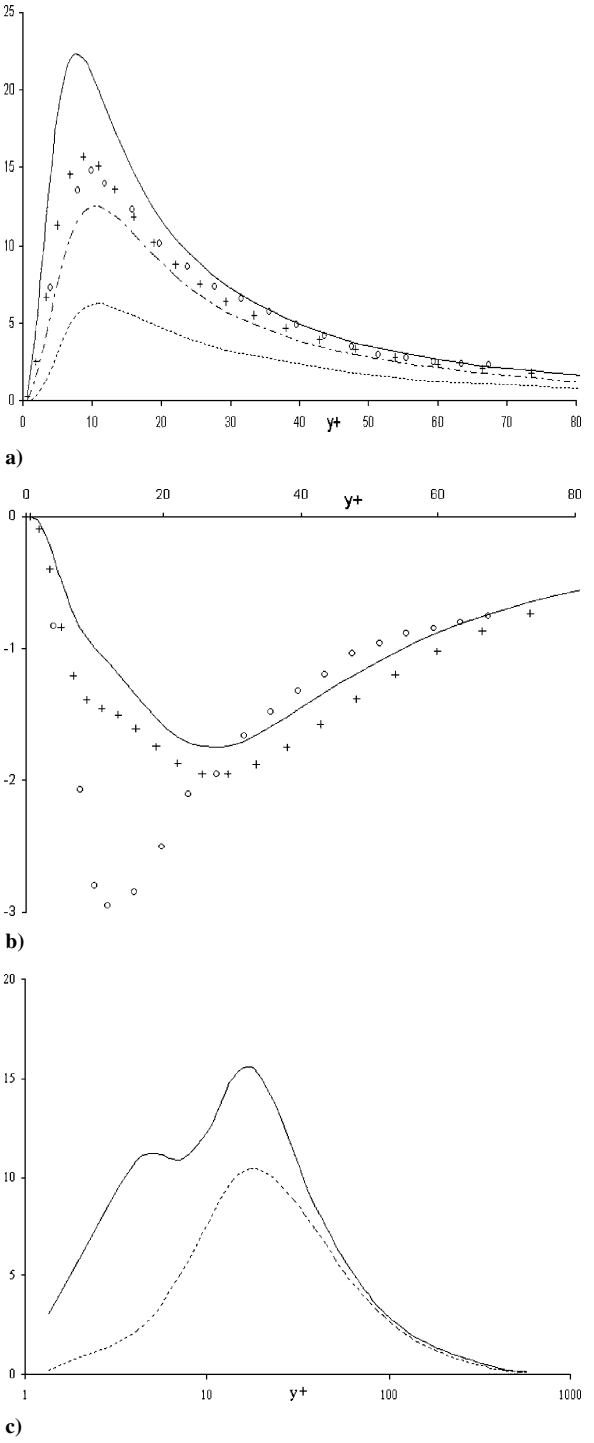

Fig. 9 Plane-averaged a) SGS dissipation, b) backscatter for case 1, and c) isotropic dissipation for case 3, normalized by u_τ, ν, and δ: — · —, SM; – – –, DSM; ——, AM^a; +, AM^b; and ○, DNS.[14]

performs much better. For the other two components both AM and DSM underpredict the flatness at the wall; this might be caused by substantial contribution of subgrid-scale motion near the wall. In the region away from the wall, the flatness values converge to three, which corresponds to the value of a Gaussian distribution. Grid refinement improves the profile in case 1 (regarded as the low-Reynolds-number effect), but not much in case 2, as expected.

As shown in Fig. 9, the net dissipation provided by all of the models agrees with the DNS results qualitatively as they peak at $y+ = 12$. In terms of magnitude, the AM is most dissipative and produces twice the dissipation as that of SM and about four times that of the DSM. The AM dissipation is comparable to the values reported by Terracol and Sagaut[39] (for cases 1 and 3) using the

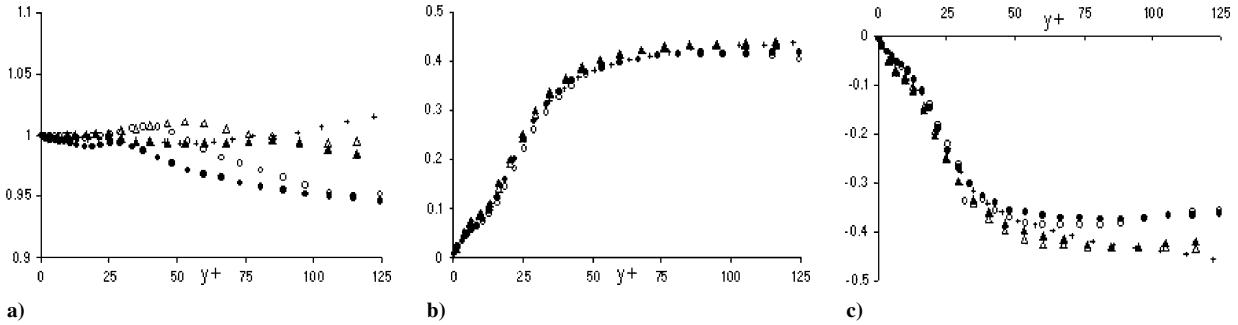

Fig. 10 Subgrid dissipation provided by AM, Eq. (2) where a) c_f (first term), b) c_L (second term), and c) c_b (third term): ○, case 1; △, case 2; +, case 3; and (SOLIDS), AM^b.

rational large eddy simulation method and Winckelmans et al.[20] (for case 2) using the tensor-diffusivity model (or the MM). By comparison with the DNS values reported by Piomelli et al.[14] for case 1, we can observe from Fig. 9a that DSM is underdissipative, whereas the algebraic model is overdissipative and SM shows the best agreement. The fine-grid results AM^b, however, show very good agreement with the DNS results.

The results also demonstrate the capability of the AM in producing backscatter via the third term of Eq. (2), although the amount of backscatter is slightly less than that obtained by Terracol and Sagaut.[39] Figure 9b shows that AM provides backscatter realistically away from the wall, but fails to predict its value near the wall. The backscatter peaks at $y+=30$ compared to $y+=12$ predicted by DNS result, which is a result of the use of an ad hoc Van Dreist damping function. The backscatter effect is reflected in the isotropic part of SGS dissipation, which should exhibit negative values in the buffer layer region.[15] Although negative values are not obtained by any of the models, the algebraic model does give a pronounced kink in the sublayer region as shown in Fig. 9c. Analysis of the energy transfer by AM terms shows that near the wall the eddy-viscosity term dominates over the other two terms and is responsible for most of the dissipation. The Leonard's term produces forward scatter nearly equal to the backscatter throughout the channel. Figure 10 displays the energy-transfer coefficients by the model terms in Eq. (2). The energy-transfer coefficient profiles show independence over the range of Reynolds numbers, as expected.

V. Free-Shear Flows

The prototypical free-shear flows studied here are the temporal planar jet and mixing layer. The flows considered are periodic along the spanwise and streamwise directions. The filtered Navier–Stokes equations are solved using a pseudospectral method employing Fourier series in the homogeneous directions and Chebyshev's polynomials along the inhomogeneous normal direction. The momentum equations are solved using a fractional step method, which involves splitting the equations into three steps. The solution of the resulting Poisson's equation is obtained using the collocation diagonalization method. Further, the infinite normal direction is algebraically mapped onto the finite domain.[41] The domain lengths considered in the simulations are the same as those in the DNS.[42,43] The simulations were started from a laminar velocity profile superimposed with normalized random phase perturbations (compare to Ansari[42] for more details).

The simulations are performed using SM, DSM, MM, and AM models discussed in the earlier section. Simulation is also performed without any model, referred to as NM. The filter width Δ is computed based on grid size as $(\Delta_x \Delta_z \Delta_y)^{1/3}$, which leads to inhomogeneous filter width in the wall-normal direction. In this paper the performance of the models in the fully developed turbulent state is studied. The results are compared with the DNS results of Ansari[42,43] at a particular instant of time. The LES results have been averaged along the homogeneous streamwise and spanwise directions to obtain mean values, and no time averaging is performed. The fluctuating velocity field is computed based on these mean values.

A. Jet Flow

The jet-flow simulation was performed for Reynolds number Re equal to 1319 based on centerline velocity and jet half-width, which corresponds to the DNS case of Ansari.[42] An initial jet half-width δ_0 of 1 and centerline velocity U_0 of 1 were chosen. The simulations were performed on two grid sizes: $32 \times 49 \times 32$ and $32 \times 65 \times 32$ along streamwise, normal, and spanwise directions, respectively, which are about four times coarser than the DNS grid requirement of $128 \times 257 \times 128$. Both the streamwise and spanwise domain lengths were $16\pi/2.65$, which is the same as that of the DNS[3,42] simulation. The turbulent state of the flow was identified by the quasi-steady value of the turbulent kinetic energy. The vorticity contours show the formation of Kelvin–Helmholtz structures at the two jet edges. These vortices break and merge with each other eventually leading to a fully developed small-scale turbulent structure. The development of the jet from the laminar to turbulent region depends on the subgrid model, and as expected the DSM adjusts to the transition better than the constant coefficient models. Postprocessing of the results in between $tU_0/\delta_0 = 95$ and 105 showed the self-similar behavior of the flow. The results presented here are at time $tU_0/\delta_0 = 100$, which is the same time at which DNS data were reported.[42]

The mean velocity profiles indicate that all of the models overestimate the jet half-width (about 2%) except for DSM, which correlates well with the DNS value in the fine-grid case. However, on the coarse-grid case the nature was reversed, and DSM overestimates the DNS value by about 1.5%. The plot of mean velocity profile (Fig. 11) shows that all of the models underpredict the maximum mean streamwise velocity. On the coarse grid SM performs the best, followed by DSM, AM, MM, and NM. On the fine grid the NM case is close to the DNS value, whereas the additional dissipation from the SGS models leads to an underprediction. DSM results are close to the NM results; this is because the SGS dissipation by DSM is much smaller than the other models (discussed next).

Profiles of turbulence intensity are presented in Fig. 12 for the fine grid. As before, the anisotropic components of the intensities are compared (taking into account both resolved and subgrid contibution) with those of DNS data. The DSM underestimates the intensities in both the grid resolutions, especially in the fine-grid case, where the results are very similar to the NM. In fact for the normal component the intensities are even smaller than the NM. On the coarse grid NM overestimates the streamwise and normal components, and the results are reasonable for other components. SM performs better for the streamwise component on fine grid, but for other components does not perform that well. Both AM and MM overestimate the intensities on fine grid, but are better on coarse grid. However, the AM results capture the profile better. The shear-stress profile as shown in Fig. 12d is predicted better by the AM, whereas the DSM predicts the least stress, which is comparable to NM. The MM results are of the order of the AM, whereas SM has an intermediate behavior. Comparison of the (SGS) shear stress shows that AM provides the highest most shear-stress levels followed by MM, SM, and DSM.

With regard to energy-transfer mechanisms, the results show that the DSM is least dissipative, with wide fluctuations in the dissipation spectra, owing to the variation of the model coefficient. SM is

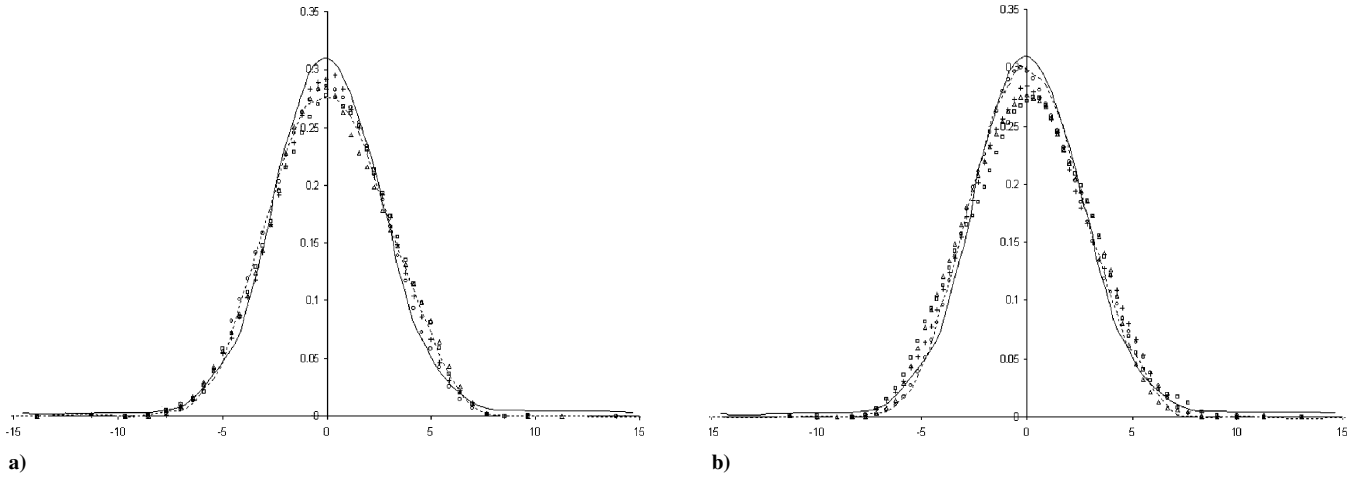

Fig. 11 Mean streamwise velocity profile along normal direction at $U_0t/\delta_0 = 100$ for the jet flow with a) coarse grid and b) fine grid: ——, DNS[42]; – – –, NM; +, SM; ○, DSM; □, MM; and Δ, AM.

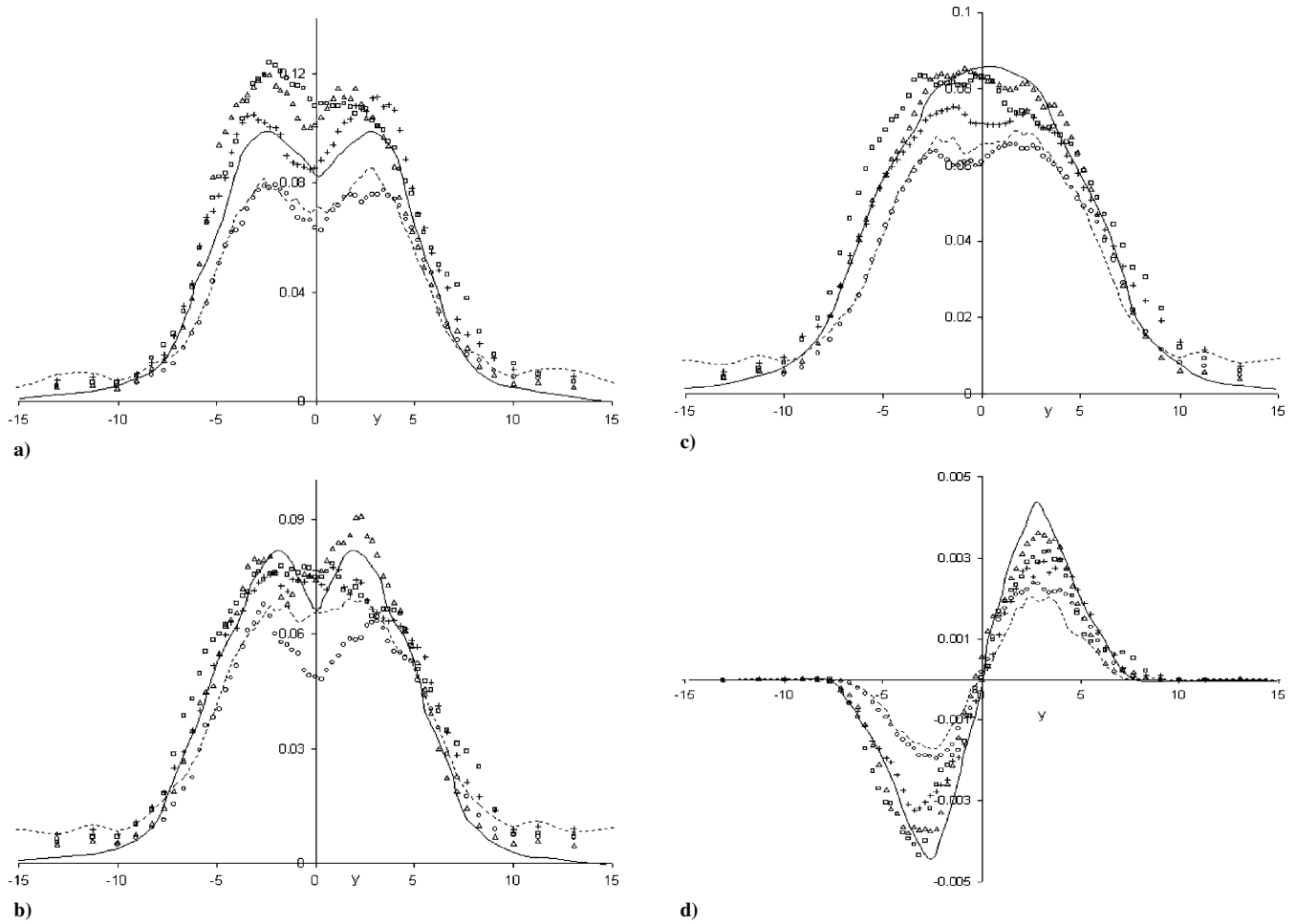

Fig. 12 Turbulence intensities: a) streamwise velocity fluctuation u', b) spanwise velocity fluctuation v', c) normal velocity fluctaution w', and d) Reynold's shear sress ($\langle u'v' \rangle$) profile on fine grid. Same keys as in Fig. 11.

slightly more dissipative than the DSM. However, both MM and AM are most dissipative (about 2.5 times more than DSM). The contribution of the AM terms to SGS dissipation is presented as energy-transfer coefficients in Fig. 13. It is evident that the third term in the model leads to explicit backscatter. The transfer coefficients are nearly constant for both the grid resolutions throughout the jet width. The amount of backscatter obtained by the AM is much lower than the value of 40% as reported by Akhavan et al.[3] Their study considered the backscatter across the cutoff (for sharp cutoff filter), which has not been considered explicitly in the AM.[4] However, the amount of backscatter in the region away from cutoff was reported to be about 10% (for the mixing layer)[32] comparable to the value obtained here.

B. Mixing Layer

The turbulent mixinglayer case is simulated for an initial Reynolds number of $Re_\delta = 220$ (defined based on $\Delta U = 2U_0$ velocity difference between two streams and δ_0 the initial momentum thickness). For the computations performed here, $U_0 = 1$ and

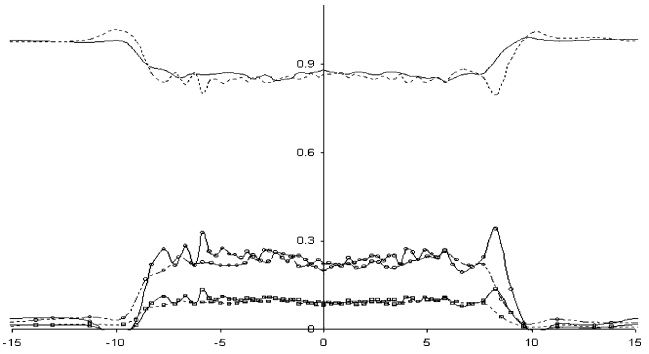

Fig. 13 Energy-transfer coefficients profile in jet flow: ——, coarse grid; – – –, fine grid; no symbol, c_f; ○, c_l; and □, c_b.

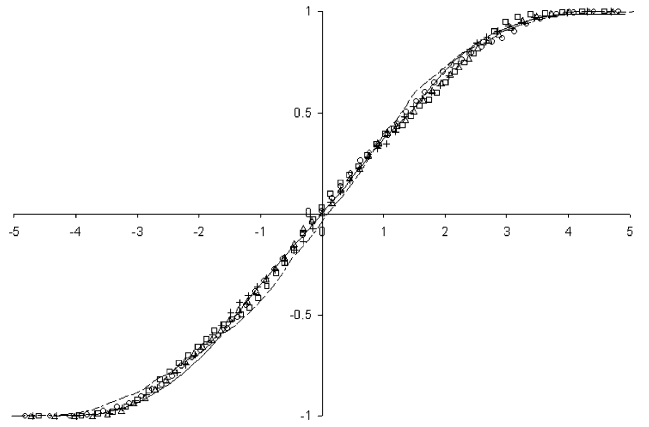

Fig. 14 Mean streamwise velocity profile normalized by U_0 at $\Delta Ut/\delta_0 = 400$ along normal direction normalized by δ_m for the mixing layer: ——, DNS[43]; – – –, NM; +, SM; ○, DSM; □, MM; and Δ, AM.

$\delta_0 = 1$, and the quiescent flow velocities are ± 1. The simulation was performed only on a single grid resolution of $32 \times 65 \times 32$ as compared to DNS grid resolution of $512 \times 257 \times 256$. The streamwise and spanwise domain lengths in this cases are $16\pi/0.446$ and $16\pi/0.8$, respectively, which are the same as that of the reference DNS.[43] The simulation undergoes transition leading to the growth of the momentum thickness δ_m, which has a slope of 0.003 in the laminar region and about 0.018 in the turbulent region. The vorticity contours show the commonly observed rollup of fundamental instability modes and successive pairing at the interface of the opposite moving fluids. The results are compared with the DNS results at $\Delta Ut/\delta_0 = 400$, where the flow has achieved a fully developed turbulent state. The self-similar characteristics of the flow were confirmed by postprocessing the results at a number of successive time instants. The plot of the mean streamwise profile (Fig. 14) shows that the results from all of the models collapse on the DNS data and provide a good mean profile. The most significant deviation is apparent for the NM case.

Figure 15 presents the plane-averaged turbulence intensities (anisotropic components as in the jet-flow case), where all of the models show a similar nature, but the NM case deviates from the DNS values most significantly. Overall, SM overpredicts the highest stress levels and DSM the lowest. Both MM and AM have an intermediate behavior between these two models. The MM predicts a better profile, especially for the normal component. For the turbulent shear-stress profile SM does not correlate well with the DNS data, and DSM fails to show a definite peak. The AM also predicts a higher value of the stress, but shows a better profile than the SM. MM predicts a smaller value than AM, but has a wider profile. The SGS shear-stress profile reveals that it has the same nature as that of Reynolds stress (also observed in the jet flow), with maximum stress produced by AM and least by SM.

As shown in Fig. 16a, both the MM and AM provide almost equal levels of dissipation, about 1.6 times as much as DSM. The SM is found to be least dissipative and almost half of the AM. The large variations in the DSM dissipation are because of the dynamic model

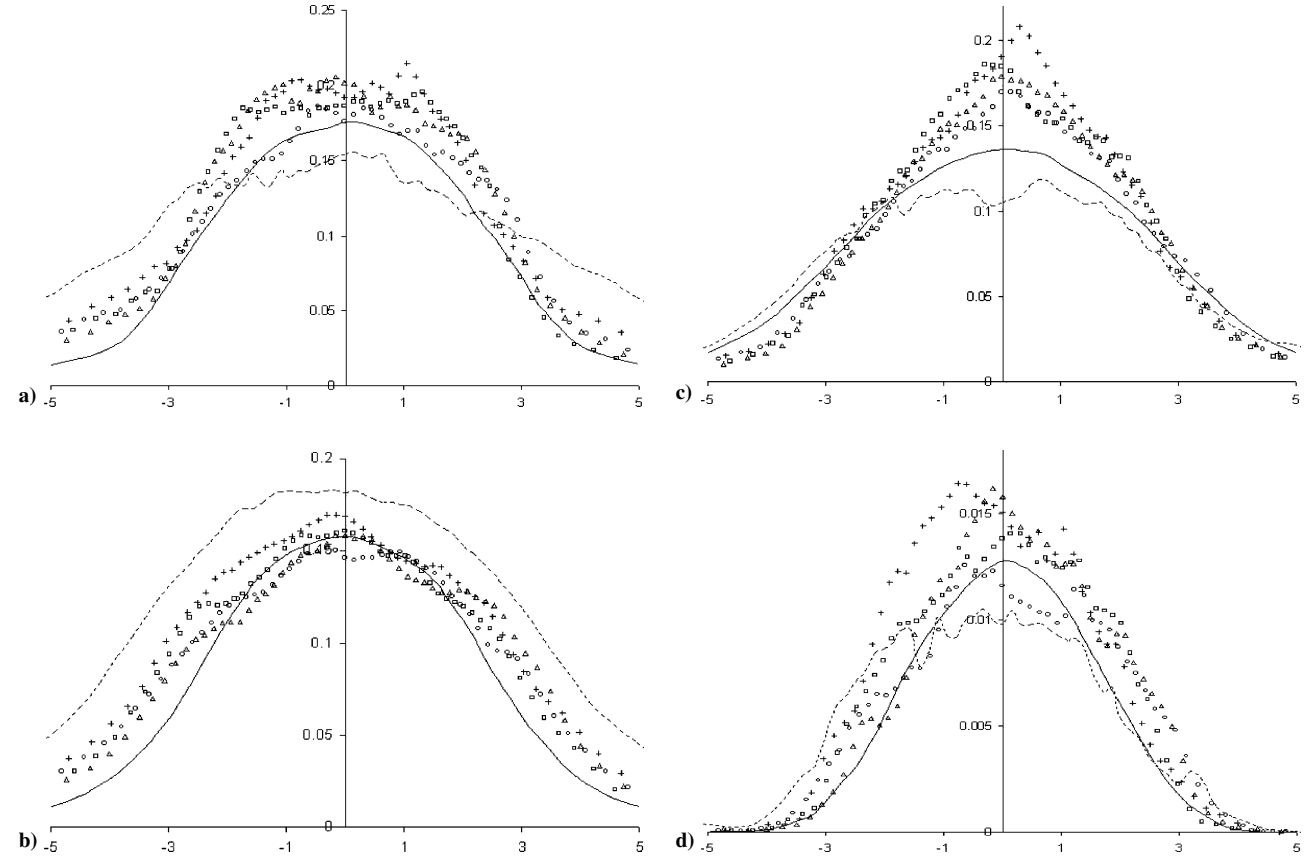

Fig. 15 RMS profile of fluctuating velocity components a) u', b) v', c) w', and d) Reynold's stress ($\langle u'v' \rangle$), normalized by ΔU along normal direction normalized by δ_m. Same keys as in Fig. 14.

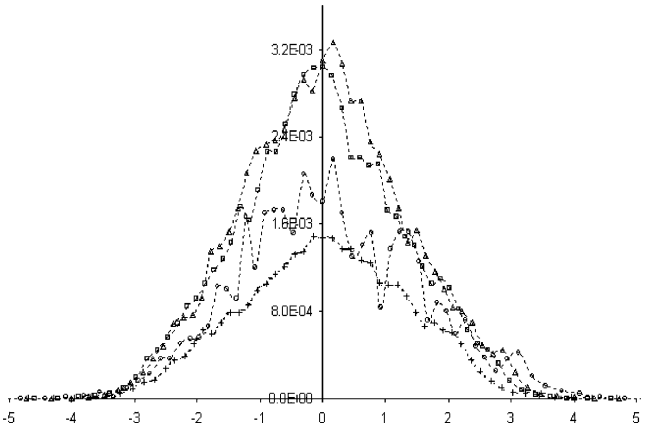

a)

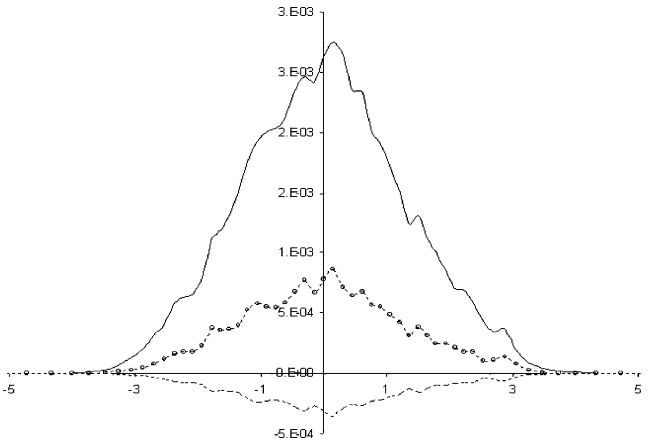

b)

Fig. 16 Mixing layer: a) SGS dissipation profile by various models with same keys as in Fig. 14 and b) dissipation by AM, Eq. (2): ——, first term (forward scatter); – – –, third term (backscatter); and – ○ –, second term (Leonard's).

coefficients in the mixing layer. Again, the AM leads to backscatter independently via the third term in the model. The amount of energy dissipation via the model terms is presented in Fig. 16b. The energy-transfer coefficients show a nearly constant value throughout the mixing layer (figure not presented) and are close to that obtained from the jet-flow case. The amount of backscatter produced by AM is in good agreement with other numerical results (compare with Vreman et al.[28] and Horiuti[25]).

Vreman et al.[28] performed simulation using various variants of MM and found that none of the models were able to account for backscatter properly in the mixing-layer simulation. However, the free-shear flow results presented here show that AM provides backscatter independently (from the third term in model) and adequately. The energy-transfer coefficients in both the free-shear cases are in good agreement with each other (presented in Table 2), which emphasizes that the subgrid-scale energy transfer occurs independent of the mean flow, as expected.

VI. Conclusions

The algebraic model has been applied to an array of LES test cases including isotropic turbulence, wall-bounded channel flow, and free-shear flows. The mean and turbulent flow quantities were compared to the commonly used subgrid-stress models such as Smagorinsky, dynamic and mixed models, and also with DNS data. For the isotropic decaying case all of the models perform equally well in depicting subgrid dissipation, but the algebraic model appears to show a better energy-transfer mechanism. In the forced isotropic case the algebraic model provided the best Kolmogrov's constant profile followed by mixed and Smagorinsky model. For the wall-bounded turbulence, both algebraic and dynamic models perform equally well for the mean flow quantities, but the algebraic model agrees better with DNS for the higher-order statistics of the flow. The algebraic model performed consistently well in both jet and mixing-layer flows.

The most important aspect of the algebraic model is its capability to represent backscatter of enegy explicitly. The amount of backscatter predicted by the algebraic model is consistent with the DNS predictions for all cases. The backscatter coefficients were also found to be independent of grid resolution and Reynolds number. The energy-transfer coefficients do vary considerably, however, for different flows. The algebraic model has constant model coefficients and is based only on the first-order derivative terms. It is therefore numerically inexpensive (requires about 3% more CPU time than Smagorinsky model compared to 12% required by dynamic Smagorinsky model). Because of the better energy-transfer capability and simple form of the model, the algebraic model shows potential to be a suitable candidate for complex engineering applications.

In its current form however, the model still suffers from some drawbacks, such as the use of the ad hoc wall damping function, and inability to adjust to transitional flows. These drawbacks of the model can be most easily addressed by computing the model coefficients dynamically. This would improve accuracy at the cost of additional numerical expense. A dynamic algebraic model is currently under investigation.

References

[1]Sarghini, F., Piomelli, U., and Balaras, E., "Scale-Similar Models for Large-Eddy Simulations," *Physics of Fluids A*, Vol. 11, No. 6, 1999, pp. 1596–1607.

[2]Domaradzki, J. A., and Saiki, E. M., "Backscatter Models for Large-Eddy Simulations," *Theoretical and Computational Fluid Dynamics*, Vol. 9, No. 2, 1997, pp. 75–83.

[3]Akhavan, R., Ansari, A., Kang, S., and Mangiavacchi, N., "Sugrid-Scale Interactions in a Numerically Simulated Planar Jet and Implications for Modeling," *Journal of Fluid Mechanics*, Vol. 408, 2000, pp. 83–120.

[4]Bhushan, S., and Warsi, Z. U. A., "Large Eddy Simulation of Turbulent Channel Flow Using an Algebnraic Model," *International Journal for Numerical Methods in Fluids*, Vol. 49, No. 5, 2005, pp. 489–519.

[5]Warsi, Z. U. A., *Fluid Dynamics, Theoretical and Computational Approaches*, 3rd ed., Taylor and Francis, Boca Raton, FL, 2005, Sec. 6.35.

[6]Leslie, D. C., and Quarini, G. L., "The Application of Turbulence Theory to the Formulation of Subgrid Modeling Procedures," *Journal of Fluid Mechanics*, Vol. 91, 1979, pp. 65–91.

[7]Schilling, O., and Zhou, Y., "Analysis of Spectral Eddy Viscosity and Backscatter in Incompressible, Isotropic Turbulence Using Statistical Closure Theory," *Physics of Fluids*, Vol. 14, No. 3, 2002, pp. 1244–1258.

[8]Chasnov, J., "Simulation of the Kolmogorov Inertial Subrange Using an Improved Subgrid Model," *Physics of Fluids A*, Vol. 3, No. 1, 1991, pp. 188–200.

[9]Lesieur, M., *Turbulence in Fluids*, Martinus Nijhoff Publishers, Dordrecht, The Netherlands, 1987, Chap. 5.

[10]Schumann, U., "Stochastic Backscatter of Turbulence Energy and Scalar Variance by Random Subgrid-Scale Fluxes," *Proceedings of Royal Society of London, A*, Vol. 451, 1941, pp. 293–318.

[11]Pope, S. B., *Turbulent Flows*, Cambridge Univ. Press, Cambridge, England, U.K., 2000, Chap. 13.

[12]Lilly, D. K., "A Proposed Modification of the Germano Subgrid-Scale Closure Method," *Physics of Fluids A*, Vol. 4, No. 3, 1992, pp. 633, 634.

[13]Meneveau, C., and Katz, J., "Scale-Invariance and Turbulence Models for Large-Eddy Simulations," *Annual Review of Fluid Mechanics*, Vol. 32, 2000, pp. 1–32.

[14]Piomelli, U., Cabot, W. H., Moin, P., and Lee, S., "Subgrid-Scale Backscatter in Turbulent and Transitional Flows," *Physics of Fluids A*, Vol. 3, No. 7, 1991, pp. 1766–1771.

[15]Hartel, C., and Kleiser, L., "Analysis and Modelling of Subgrid-Scale Motion in near Wall Turbulence," *Journal of Fluid Mechanics*, Vol. 356, 1998, pp. 327–352.

[16]Carati, D., Ghosal, S., and Moin, P., "On the Representation of Backscatter in Dynamic Localization Models," *Physics of Fluids*, Vol. 7, No. 3, 1995, pp. 606–616.

[17]Piomelli, U., and Yu, Y., "Subgrid-Scale Energy Transfer and near-Wall Turbulence Structure," *Physics of Fluids*, Vol. 8, No. 1, 1996, pp. 215–224.

[18]Dunn, D. C., and Morrision, J. F., "Anisotropy and Energy Flux in Wall Turbulence," *Journal of Fluid Mechanics*, Vol. 491, 2003, pp. 353–378.

[19]Bardina, J., "Improved Turbulence Models Based on Large Eddy Simulation of Homogeneous, Incompressible Turbulent Flows," Ph.D. Dissertation, Dept. of Mechanical Engineering, Stanford Univ. Stanford, CA, 1983.

[20]Winckelmans, G. S., Wray, A. A., Vasilyev, O. V., and Jeanmart, H., "Explicit-Filtering Large-Eddy Simulation Using the Tensor-Diffusivity Model Supplemented by a Dynamic Samgorinsky Term," *Physics of Fluids A*, Vol. 5, No. 13, 2001, pp. 1385–1403.

[21]Carati, D., Winckelmans, G. S., and Jeanmart, H., "On Modelling of the Subgrid-Scale and Filtered-Scale Stress Tensors in Large-Eddy Simulation," *Journal of Fluid Mechanics*, Vol. 441, 2001, pp. 119–138.

[22]Domaradzki, J. A., and Adams, N. A., "Direct Modelling of Subgrid Scales of Turbulence in Large Eddy Simulation," *Journal of Turbulence*, Vol. 3, No. 24, 2002.

[23]Iliescu, T., and Fischer, P. F., "Large Eddy Simulation of Turbulent Channel Flows by the Rational Large Eddy Simulation Model," *Physics of Fluids*, Vol. 15, No. 10, 2003, pp. 3036–3047.

[24]Brun, C., and Friedrich, R., "Modeling the Test SGS Tensor T_{ij}: An Issue in the Dynamic Approach," *Physics of Fluids A*, Vol. 13, No. 8, 2001, pp. 2373–2385.

[25]Horiuti, K., "A New Dynamic Two-Parameter Mixed Model for Large-Eddy Simulation," *Physics of Fluids*, Vol. 9, No. 11, 1997, pp. 3443–3464.

[26]Menon, S., Yeung, P. K., and Kim, W. W., "Effect of Subgrid Models on the Computed Interscale Energy Transfer in Isotropic Turbulence," *Computers and Fluids*, Vol. 25, No. 2, 1996, pp. 165–180.

[27]Leonard, A., "Energy Cascade in Large-Eddy Simulations of Turbulent Fluid Flows," *Advances in Geophysics*, Vol. 18, 1974, pp. 237–248.

[28]Vreman, B., Geurts, B., and Kuerten, H., "Large-Eddy Simulation of Turbulent Mixing Layer," *Journal of Fluid Mechanics*, Vol. 339, 1997, pp. 357–390.

[29]Kang, H. S., Chester, S., and Meaneveau, C., "Decaying Turbulence in an Active-Grid-Generated Flow and Comparisions with Large-Eddy Simulation," *Journal of Fluid Mechanics*, Vol. 480, 2003, pp. 129–160.

[30]Kosovic, B., "Subgrid Scale Modelling for the Large-Eddy Simulation of High-Reynolds-Number Boundary Layer," *Journal of Fluid Mechanics*, Vol. 336, 1997, pp. 151–182.

[31]Mohseni, K., Kosovic, B., Shkoller, S., and Marsden, J. E., "Numerical Simulations of the Lagrangian Averaged Navier–Stokes Equations for Homogeneous Isotropic Turbulence," *Physics of Fluids*, Vol. 15, No. 2, 2003, pp. 524–544.

[32]Geurts, B. J., and Holm, D. D., "Alpha-Modeling Strategy for LES of Turbulent Mixing Layer," *Turbulent Flow Computation (Fluid Mechanics and its Application)*, Vol. 66, Kluwer Academic, Boston, 2002, pp. 237–278.

[33]Collis, S. S., "Monitoring Unresolved Scales in Multiscale Turbulence Modeling," *Physics of Fluids*, Vol. 13, No. 6, 2001, pp. 1800–1806.

[34]Chang, Y., "Approximate Models for Optimal Control of Turbulent Channel Flow," Ph.D. Dissertation, Dept. of Mechanical Engineering and Materials Science, Rice Univ., Houston, TX, 2000.

[35]Rogallo, R. S., "Numerical Experiments in Homogeneous Turbulence," NASA TM-73203, 1981.

[36]Stefano, G. S., and Vasilyev, O. V., "Sharp Cut-off Versus Smooth Filtering in Large Eddy Simulation," *Physics of Fluids*, Vol. 14, No. 1, 2002, pp. 362–369.

[37]Comte-Bellot, G., and Corrsin, S., "Simple Eulerian Time Correlation of Full and Narrow-Band Velocity Signals in Grid-Generated, 'Isotropic' Turbulence," *Journal of Fluid Mechanics*, Vol. 48, 1971, pp. 273–337.

[38]Moser, R. D., Kim, J., and Mansour, N. N., "Direct Numerical Simulation of Turbulent Channel Flow up to $Re_\tau = 590$," *Physics of Fluids*, Vol. 11, No. 4, 1999, pp. 943–945.

[39]Terracol, M., and Sagaut, P., "Multilevel-Based Dynamic Approach for Subgrid-Scale Modeling in Large Eddy Simulation," *Physics of Fluids*, Vol. 15, No. 12, 2003, pp. 3671–3682.

[40]Kim, J., Moin, P., and Moser, R., "Turbulence Statistics in Fully Developed Channel Flow at Low Reynolds Number," *Journal of Fluid Mechanics*, Vol. 177, 1987, pp. 133–165.

[41]Peyret, R., "Spectral Methods for Incompressible Viscous Flow," *Applied Mathematical Sciences*, Vol. 148, Springer, 2001, Chap. 3.

[42]Ansari, A., "Small-Scale Dynamics and Subgrid Interactions in Turbulent Shear Flows," Ph.D. Dissertation, Dept. of Atmospheric, Oceanic and Space Sciences, Univ. of Michigan, Ann Arbor, MI, 1993.

[43]Ansari, A., "Self-Similarity and Mixing Characteristics of Turbulent Mixing Layer," *Physics of Fluids*, Vol. 9, No. 6, 1997, pp. 1714–1728.

P. Givi
Associate Editor